A Wiener-Hopf-Type Analysis of Microstrips Printed on Uniaxial Substrates: Effects of the Substrate Thickness

George A. Kyriacou, *Member, IEEE,* and John N. Sahalos, *Senior Member, IEEE*

Abstract—A Wiener-Hopf-type analysis of the canonical problem of a TEM wave obliquely incident at the edge of the truncated upper conductor of a parallel plate waveguide loaded with a uniaxial anisotropic dielectric is presented. A numerical integration scheme as well as a thin substrate approximation for the reflection coefficient is given. The influence of the dielectric anisotropy and the slab thickness on the reflection coefficient and the edge admittance are investigated. Numerical results show the importance of the dielectric anisotropy and the expected effects in microstrip applications.

I. INTRODUCTION

A LOT OF substrate materials used in the fabrication of microstrip lines or patch antennas exhibit a dielectric anisotropy. The anisotropy is either intrinsic of the material or artificially caused by the substrate manufacturing process. Moreover, crystalline substrates are preferable in some applications because they have certain advantages over ceramics, such as higher homogeneity, lower losses, and lower variations from sample to sample. Examples of monocrystalline dielectrics suggested for use as substrates include: monocrystalline sapphire, with relative permittivity along the principal crystal axis $\varepsilon_{||}$ =11.6, and perpendicular to that $\varepsilon_\perp$ =9.4 and monocrystalline magnesium fluoride with $\varepsilon_{||}$ =4.826 and $\varepsilon_\perp$ =5.5. Ceramic Impregnated teflon, like Epsilam 10 with $\varepsilon_{||}$ =10.2 and $\varepsilon_\perp$ =13.0, is an example of artificially caused uniaxial anisotropy. The substrate anisotropy must be taken into account because it can be used to improve the performance of printed lines and antennas.

Although many studies have been presented on transmission lines (see an excellent review article written by Alexopoulos [1] and the references therein), there are rather few works (e.g., [2]–[4], [12]) in the field of antennas. Also, some recent works are studying the characterization of microstrip discontinuities patterned on uniaxial anisotropic substrates (e.g., [13]). At the same time the interest of the investigators is extending toward the inclusion of an also uniaxial superstrate [14], [15]. In our previous study [4], the Wiener-Hopf technique has been applied to solve the canonical problem of a TEM wave obliquely incident on the truncation of the upper plate of a parallel plate waveguide loaded with a uniaxially anisotropic

dielectric slab. Moreover, the integrals arising from the solution of the Wiener-Hopf equations have been approximated in closed form for the usual case of electrically thin substrates. This work, [4], could be considered as an extension of the studies by Kuester and Chang [5], [6]. The validity of [4] has been tested in two ways. First, letting the anisotropy ratio be equal to one (or $\varepsilon_{||} = \varepsilon_\perp = \varepsilon_r$). It was verified that the infinite integrals and the closed form expressions were exactly reduced to the corresponding ones of the isotropic problem [5], [6]. Second, by comparing the numerical results for the resonant frequency of rectangular patch antennas with those given by Nelson [3] and Pozar [2]. It was found that they were in very good agreement.

Our present effort has to do with the numerical evaluation of the infinite Sommerfeld-type integrals involved in the field expressions and the application of the theory in the analysis of microstrip antennas. The numerical integration will show the limits of the thin substrate approximation and will help investigate new applications with electrically thick substrates.

In order for this paper to be self-sustained, we first summarize the formulation given in [4].

II. FORMULATION OF THE WIENER-HOPF EQUATIONS FOR THE UNIAXIAL SUBSTRATE

Consider a vertically polarized TEM wave obliquely incident (at an angle Φ) on the edge of the truncated upper conductor of an otherwise infinite parallel plate waveguide loaded with an infinitely extended uniaxial dielectric slab (see Fig. 1). The uniaxial dielectric is assumed to be fabricated (or cut) with its optical axis perpendicular to the conductor plane (along the z-axis). Let the relative dielectric constant along the optical axis be $\varepsilon_z = \varepsilon_{||}$ and the one transverse to the optical axis be $\varepsilon_x = \varepsilon_y = \varepsilon_\perp$. The corresponding refraction indices are $n_{||} = \sqrt{\mu_r \varepsilon_{||}}$ and $n_\perp = \sqrt{\mu_r \varepsilon_\perp}$. The vertically polarized TEM wave can be expressed as $E_z^i = \exp[jk_0(\xi x - \alpha y)]$, where $\alpha = n_{||} \sin \varphi$, $\xi = n_{||} \cos \varphi$ and k_0 is the wavenumber in free space. The scattered field (reflected and radiated) by the edge can be obtained with the adoption of the continuous Fourier spectrum in conjunction with the Wiener-Hopf technique.

In order to get an analytical solution, Maxwell equations are first simplified by considering: 1) time harmonic fields of the form $e^{j\omega t}$, 2) propagation of the incident and scattered field in the y-direction, as $e^{-jk_0\alpha y}$, which gives $\partial/\partial y \rightarrow -jk_0\alpha$, and 3) typical Fourier transform pair $\{\tilde{f}(\lambda), f(x)\}$ used in

Wiener-Hopf approaches in the x-direction (perpendicular to the edge). The transformed function $\tilde{f}(\lambda)$ is considered as the summation of two functions $\tilde{f}(\lambda) = \tilde{f}_-(\lambda) + \tilde{f}_+(\lambda)$ defined in the intervals $x \in (-\infty, 0)$ and $(0, +\infty)$, respectively, where $\tilde{f}_-(\lambda)$ and $\tilde{f}_+(\lambda)$ are analytic in the lower and the upper half of the complex λ-plane correspondingly. This transform gives the simplification $\partial/\partial x \rightarrow -jk_0\lambda$.

Furthermore, the "hybrid mode" technique is applied by considering the scattered field to be given as a superposition of LSE or TE$_z$ (with $E_z = 0$) and LSM or TM$_z$ (with $H_z = 0$) modes. Using all the above simplifications the field components are expressed in terms of $\tilde{H}_z^{\text{TE}_z}$ and $\tilde{E}_z^{\text{TM}_z}$, also the wave equations for these two z-components are obtained. Applying the radiation condition as well as the boundary conditions for the tangential electric field at the infinite metallic ground plane ($z = 0$) and at the air-dielectric interface ($z = d$), the scattered field expressions are given as follows:

Air region $(z > d)$

$$\tilde{E}_z^s = E_0 e^{-k_0 u_0(z-d)} \quad \text{and} \quad \tilde{H}_z^s = H_0\, e^{-k_0 u_0(z-d)} \quad (2a)$$

$$\tilde{E}_t^s = \frac{j}{\alpha^2 + \lambda^2}\left\{ (\lambda\hat{x} - \alpha\hat{y}) u_0 E_0 - j\zeta_0(\alpha\hat{x} + \lambda\hat{y})H_0 \right\}$$
$$\times e^{-k_0 u_0(z-d)} \quad (2b)$$

$$\tilde{H}_t^s = \frac{j}{\alpha^2 + \lambda^2}\left\{ (\lambda\hat{x} - \alpha\hat{y}) u_0 H_0 - \frac{j}{\zeta_0}(\alpha\hat{x} + \lambda\hat{y})E_0 \right\}$$
$$\times e^{-k_0 u_0(z-d)} \quad (2c)$$

where $u_0 = \sqrt{\lambda^2 + \alpha^2 - 1}$, $\text{Re}\{u_0\} \geq 0$ and $\zeta_0 = 120\pi\ \Omega$, the characteristic impedance of free space.

Dielectric region $(z < d)$

$$\tilde{E}_z^s = E_n \frac{\cosh(k_0 u_{n2} z)}{\cosh(k_0 u_{n2} d)} \quad \text{and} \quad \tilde{H}_z^s = H_n \frac{\sinh(k_0 u_{n1} z)}{\sinh(k_0 u_{n1} d)} \quad (3a)$$

$$\tilde{E}_t^s = \frac{j}{\alpha^2 + \lambda^2}\left\{ -\left(\frac{\varepsilon_{||}}{\varepsilon_\perp}\right)(\lambda\hat{x} - \alpha\hat{y})\frac{u_{n2}\sinh(k_0 u_{n2} z)}{\cosh(k_0 u_{n2} d)} \right.$$
$$\times E_n - j\zeta_0\mu_r(\alpha\hat{x} + \lambda\hat{y})$$
$$\left. \times \frac{\sinh(k_0 u_{n1} z)}{\sinh(k_0 u_{n1} d)}H_n \right\} \quad (3b)$$

$$\tilde{H}_t^s = \frac{j}{\alpha^2 + \lambda^2}\left\{ -(\lambda\hat{x} - \alpha\hat{y})\frac{u_{n1}\cosh(k_0 u_{n1} z)}{\sinh(k_0 u_{n1} d)}H_n \right.$$
$$+ j\left(\frac{\varepsilon_{||}}{\zeta_0}\right)(\alpha\hat{x} + \lambda\hat{y})$$
$$\left. \times \frac{\cosh(k_0 u_{n2} z)}{\cosh(k_0 u_{n2} d)}E_n \right\} \quad (3c)$$

where

$$u_{n1} = \sqrt{\lambda^2 + \alpha^2 - n_\perp^2}, \quad \text{and} \quad \text{Re}\{u_{n1}\} \geq 0$$

$$u_{n2} = (n_\perp/n_{||})\sqrt{\lambda^2 + \alpha^2 - n_{||}^2}, \quad \text{and} \quad \text{Re}\{u_{n2}\} \geq 0.$$

The Wiener-Hopf equations for the electric and the magnetic fields can be obtained by applying the boundary conditions for the normal to the interface electric flux density component D_z and the tangential magnetic field $\bar{H}_t$, respectively. Namely, D_z and $\bar{H}_t$ are continuous at the air dielectric interface ($z =$
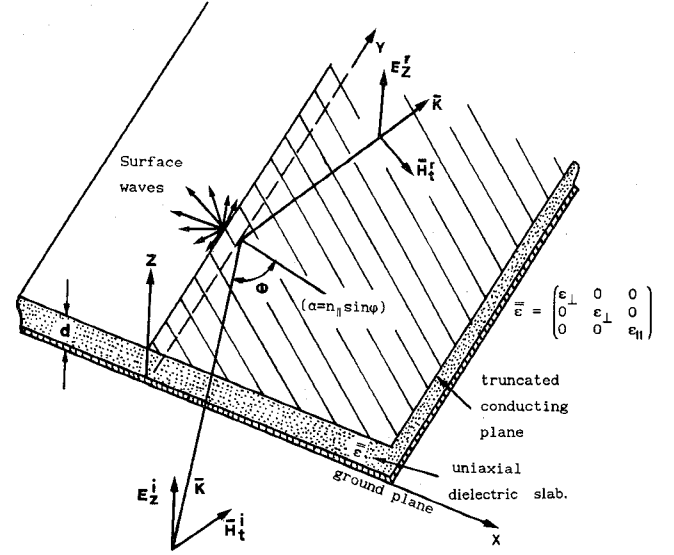

Fig. 1. A TEM wave obliquely incident on the edge of the truncated upper conductor of an infinite extend grounded uniaxial anisotropic dielectric slab.

$d, x < 0$), and discontinuous on the truncated upper conductor ($z = d, x > 0$) by the amounts of the induced surface charge $\rho^s(x)$ and current $\bar{J}_t = \hat{z}x\bar{H}$ densities, correspondingly. The electric field is

$$\tilde{E}_z^s(\lambda, z = d^+) = \varepsilon_{||}\tilde{E}_z^s(\lambda, z = d^-) - \tilde{\rho}_-^i(\lambda)/\varepsilon_0 + \tilde{\rho}_+^s(\lambda)/\varepsilon_0 \quad (4)$$

where $\tilde{\rho}_+^s(\lambda), \tilde{\rho}_-^i(\lambda)$ are the Fourier transforms of the surface charge densities, on the truncated upper conductor associated with the scattered and the incident field, respectively. $\tilde{\rho}_-^i(\lambda)$ can be explicitly found by applying the corresponding boundary condition. Likewise, the Wiener-Hopf equation for the magnetic field is

$$\tilde{H}_z'^s(\lambda, z = d^+) - \tilde{H}_z'^s(\lambda, z = d^-) = \tilde{j}_+(\lambda) \quad (5)$$

where $\tilde{H}_z'^s = \bar{\nabla}_t \cdot \tilde{H}_t'^s$ and $\tilde{j}_+(\lambda)$ is the Fourier transform of the quantity $-\bar{\nabla}_t \cdot [\hat{z} \times \bar{J}_t(x)]$.

In a way similar to that of [5]–[7], two functions $\tilde{F}_-(\lambda)$ and $\tilde{G}_-(\lambda)$ are correspondingly defined as the Fourier transform of quantities proportional to the total charge ρ_t^s and the total current J_t^s densities induced on the truncated upper conductor. The unknown field spectral amplitudes (functions) (E_0, E_n) and (H_0, H_n) appearing in (2) and (3) are then expressed through the previously established boundary conditions as

$$E_0 = \tilde{F}_-(\lambda)/u_0 \quad \text{and} \quad E_n = -\frac{\varepsilon_\perp}{\varepsilon_{||}}\frac{\tilde{F}_-(\lambda)}{u_{n2}\tanh(k_0 u_{n2} d)} \quad (6)$$

$$H_0 = j\tilde{G}_-(\lambda)/\zeta_0 \quad \text{and} \quad H_n = j\frac{\tilde{G}_-(\lambda)}{\zeta_0\mu_r}. \quad (7)$$

Finally, the Wiener-Hopf equation for the electric field takes the form

$$\tilde{F}_-(\lambda) = Q_e(\lambda)\frac{\tilde{\rho}_+^s(\lambda) - \tilde{\rho}_-^i(\lambda)}{\varepsilon_0} \quad (8)$$

where

$$Q_e(\lambda) = \frac{u_0 u_{n2}\tanh(k_0 u_{n2} d)}{\varepsilon_\perp u_0 + u_{n2}\tanh(k_0 u_{n2} d)} \quad (9)$$

while, that for the magnetic field

$$\tilde{G}_-(\lambda) = Q_m(\lambda)\frac{\tilde{j}_+(\lambda)}{j\omega\varepsilon_0} \tag{10}$$

where

$$Q_m(\lambda) = \frac{\mu_r}{\mu_r u_0 + u_{n1}\coth(k_0 u_{n1}d)}. \tag{11}$$

For the solution of the Wiener-Hopf equations it is necessary to perform a factorization of the functions $Q_e(\lambda)$ and $Q_m(\lambda)$ into a product $Q_+(\lambda)Q_-(\lambda)$, where $Q_+(\lambda)$ is a "positive" and $Q_-(\lambda)$ is a "negative" function, in the sense that they are analytic in the upper and lower complex λ-half planes. The factorization technique, given by Mittra and Lee [8], helps to find a solution of the following form:

$$\tilde{F}_-(\lambda) = -j\frac{k_0 d}{\pi}\sqrt{n_{||}^2 - \alpha^2}\left\{\frac{\lambda + j\alpha\tanh(\Delta)}{\sqrt{n_{||}^2 - \alpha^2} - j\alpha\tanh(\Delta)}\right\}$$

$$\cdot e^{-j\left[f_e(-\lambda) + f_e\left(-\sqrt{n_{||}^2 - \alpha^2}\right)\right]/2} \tag{12}$$

$$\tilde{G}_-(\lambda) = -j\frac{k_0 d}{\pi}\sqrt{n_{||}^2 - \alpha^2}$$

$$\times \frac{\alpha \cdot e^{-j\left[f_e\left(-\sqrt{n_{||}^2 - \alpha^2}\right) + f_m(-\lambda)\right]/2}}{\sqrt{n_{||}^2 - \alpha^2} - \cosh(\Delta) - j\alpha\sinh(\Delta)} \tag{13}$$

where

$$f_e(\lambda) = j\ln\left\{\frac{\varepsilon_\perp}{\left(\frac{\varepsilon_\perp}{\varepsilon_{||}} + \varepsilon_\perp\frac{n_\perp}{n_{||}}\right)k_0 d\left(\sqrt{\alpha^2 - 1} - j\lambda\right)}\right\}$$

$$+ \frac{2\lambda}{\pi}\int_0^\infty \ln\{q_e(w)\}\frac{dw}{w^2 - \lambda^2} \tag{14a}$$

$$f_m(\lambda) = j\ln\left\{\frac{1}{(1 + \mu_r)k_0 d\left(\sqrt{\alpha^2 - 1} - j\lambda\right)}\right\}$$

$$+ \frac{2\lambda}{\pi}\int_0^\infty \ln\{q_m(w)\}\frac{dw}{w^2 - \lambda^2}. \tag{14b}$$

The functions $q_e(\lambda)$ and $q_m(\lambda)$ are

$$q_e(\lambda) = \frac{\left(\frac{\varepsilon_\perp}{\varepsilon_{||}} + \varepsilon_\perp\frac{n_\perp}{n_{||}}\right)u_0^2\tanh(k_0 u_{n2}d)}{u_{n2}[\varepsilon_\perp u_0 + u_{n2}\tanh(k_0 u_{n2}d)]} \tag{15a}$$

$$q_m(\lambda) = \frac{(1 + \mu_r)u_0}{\mu_r u_0 + u_{n1}\coth(k_0 u_{n1}d)} \tag{15b}$$

and

$$\Delta(\alpha) = \frac{\alpha}{\pi}\int_0^\infty \ln$$

$$\times \left\{\frac{\varepsilon_\perp u_0\tanh(k_0 u_{n2}d)[\mu_r u_0 + u_{n1}\coth(k_0 u_{n1}d)]}{u_{n2}[\varepsilon_\perp u_0 + u_{n2}\tanh(k_0 u_{n2}d)]}\right\}$$

$$\times \frac{d\lambda}{\lambda^2 + \alpha^2}. \tag{15c}$$

In order for the above integrals to have an efficient numerical convergence, the argument of the natural logarithm should approach unity as the integration variable (λ) goes to infinity.

This is actually true for all of them except $\Delta(\alpha)$ [see 15(c)] which, in order to satisfy these conditions, is modified to

$$\Delta(\alpha) = \frac{1}{2}\ln\left\{\frac{\varepsilon_\perp(1 + \mu_r)}{(\varepsilon_\perp/\varepsilon_{||}) + \varepsilon_\perp(n_\perp/n_{||})}\right\} + \frac{\alpha}{\pi}\int_0^\infty$$

$$\times \ln\left\{\frac{(\varepsilon_\perp/\varepsilon_{||}) + \varepsilon_\perp(n_\perp/n_{||})}{1 + \mu_r}\right.$$

$$\left.\cdot \frac{u_0\tanh(k_0 u_{n2}d)[\mu_r u_0 + u_{n1}\coth(k_0 u_{n1}d)]}{u_{n2}[\varepsilon_\perp u_0 + u_{n2}\tanh(k_0 u_{n2}d)]}\right\}$$

$$\times \frac{d\lambda}{\lambda^2 + \alpha^2} \tag{15d}$$

From the above expressions all the components of the electric and magnetic fields can be obtained through the functions $\tilde{F}_-(\lambda)$ and $\tilde{G}_-(\lambda)$ in the Fourier spectrum domain. An inverse Fourier transform is needed to get their expressions in the real space domain. This is a quite complicated task, since the field spectral components are already expressed as Sommerfeld type integrals.

Near the edge, higher-order modes are excited, but most of them are evanescent type modes and they vanish at a practically small distance. Therefore, only the propagating modes will exist at some distance from the edge. The dominant mode which always exists is again a vertically polarized TEM-reflected wave. This wave can be obtained with the help of a reflection coefficient, as

$$\Gamma_{\text{TEM}}(\alpha) = \frac{(E_z^s)_{\text{TEM}}}{(E_z^i)_{\text{TEM}}}\bigg|_{x=0}$$

$$= j\pi\frac{\tilde{F}_-\left(\lambda = \sqrt{n_{||}^2 - \alpha^2}\right)}{k_0 d\sqrt{n_{||}^2 - \alpha^2}} = e^{jX(\alpha)} \tag{16}$$

where $X(\alpha)$ after some algebraic manipulations turn out to be

$$X(\alpha) = 2\tan^{-1}\left\{\frac{\alpha\tanh(\Delta)}{\sqrt{n_{||}^2 - \alpha^2}}\right\} - f_e\left(-\sqrt{n_{||}^2 - \alpha^2}\right). \tag{17}$$

The contribution of the integral involved in the $f_e(\lambda)$ expression at the pole $w \to \lambda = +\sqrt{n_{||}^2 - \alpha^2}$ is extracted and f_e is expressed as a principal value integral more properly suited for numerical integration (since the pole singularity is extracted). That is

$$f_e\left(-\sqrt{n_{||}^2 - \alpha^2}\right) = \tan^{-1}\left(\frac{\sqrt{n_{||}^2 - \alpha^2}}{\sqrt{\alpha^2 - 1}}\right)$$

$$- \frac{2}{\pi}\sqrt{n_{||}^2 - \alpha^2}\,\text{PV}\int_0^\infty \ln\{q_e(\lambda)\}\frac{d\lambda}{\lambda^2 - (n_{||}^2 - \alpha^2)} \tag{18}$$

where for convenience the integration variable is changed from w to λ.

It is important to note that, by letting the anisotropy ratio equal to one, namely $n_\perp = n_{||} = n$ or $\varepsilon_\perp = \varepsilon_{||} = \varepsilon_r$, the expressions, either for the field components or the Wiener-Hopf equations solution, are exactly reduced to those of the isotropic case given by Chang and Kuester [5].

The TEM reflection coefficient can be calculated either by using numerical integration or the thin substrate approximation. With the knowledge of Γ_{TEM} the open end edge admittance Y_e can be evaluated

$$Y_e = G_e + jB_e = Y_0 \frac{1 - \Gamma_{\text{TEM}}}{1 + \Gamma_{\text{TEM}}}$$
$$= Y_0 \frac{1 - e^{jX(\alpha)}}{1 + e^{jX(\alpha)}} = -jY_0 \tan(X(\alpha)). \qquad (19)$$

G_e, B_e are the edge conductance and edge susceptance, respectively. Y_0 is the characteristic admittance of the parallel plate waveguide loaded with a uniaxial dielectric slab. The admittance Y_0, related to the Z-polarized TEM wave propagating in this waveguide, can be defined as the ratio of the current per unit length flowing on the conductors in the direction of propagation to the voltage developed between them. Using for simplicity the incident TEM wave components (the same result can be obtained from the scattered TEM wave), it is found that $Y_0 = |H_t^i|/(E_z^i d)$ or $Y_0 = n_{||}/(\mu_r \zeta_0 d)$.

III. SURFACE WAVES, CUTOFF FREQUENCIES, AND APPROXIMATE WAVENUMBERS

The LSE and LSM surface wave characteristic equations can be obtained by setting, respectively the denominators of Q_e and Q_m in (9) and (11) equal to zero. In order to determine their cutoff frequencies or the modes' turn on conditions, a clarifying "graphical" solution of such transcendental equations, used by many authors, e.g. [10], is applied. For the LSE modes, let us define their wavenumber α_{p_e} as $\alpha_{p_e}^2 = \lambda^2 + \alpha^2$, and let $\sqrt{n_{||}^2 - \alpha_{p_e}^2} = k_{ce}/k_0$, $\sqrt{\alpha_{p_e}^2 - 1} = h_e/k_0$, $u_{n2} = j(n_\perp/n_{||}) \cdot k_{ce}/k_0$ and $u_0 = h_e/k_0$. Using these definitions the LSE modes characteristic equation becomes

$$\frac{n_\perp}{n_{||}} k_{ce} \tan\left[\frac{n_\perp}{n_{||}} k_{ce} \cdot d\right] = \varepsilon_\perp h_e \qquad (20a)$$

Also the unknowns k_{ce} and h_e are simply related as

$$k_{ce}^2 + h_e^2 = k_0^2(n_{||}^2 - 1) \qquad (20b)$$

The above two equations must be solved simultaneously. Rearranging, we get a form more suitable for graphical solution

$$\left(k_{ce} d \frac{n_\perp}{n_{||}}\right) \tan\left[k_{ce} d \frac{n_\perp}{n_{||}}\right] = \varepsilon_\perp \frac{n_{||}}{n_\perp}\left(h_e d \frac{n_\perp}{n_{||}}\right) \qquad (20c)$$

$$\left(k_{ce} d \frac{n_\perp}{n_{||}}\right)^2 + \left(h_e d \frac{n_\perp}{n_{||}}\right)^2 = \left(k_0 d \frac{n_\perp}{n_{||}} \sqrt{n_{||}^2 - 1}\right)^2 = r_e^2. \qquad (20d)$$

In order to get a graphical representation (20c) and (20d) can be plotted (see [10] for the isotropic case) on an axis system $k_{ce} d(n_\perp/n_{||})$ versus $h_e d(n_\perp/n_{||})$. Equation (20d) represents a circle about the origin with radius r_e. Moreover, recalling the restriction $\text{Re}(u_0) \geq 0$, the valid solutions (points where the two curves intercept each other) are only those giving $h_e \geq 0$. Since the curve of (20c) passes always through the origin and is lying on the positive half plane, there is always a valid first-order solution. This solution corresponds to the first LSE mode, which is then always excited. Furthermore, as the

radius r_e becomes larger (thicker substrate $k_0 d \nearrow$ or larger anisotropy ratio $(n_\perp/n_{||}) \nearrow$), higher order LSE modes are excited. Valid solutions $(h_e \geq 0)$ are obtained for $r_e \geq p_e \pi$. The turn on condition of the p_eth mode is defined as $r_e = p_e \pi$, which gives

$$k_0 d \frac{n_\perp}{n_{||}} \sqrt{n_{||}^2 - 1} = p_e \pi \quad \text{with} \quad p_e = 0, 1, 2, \ldots \qquad (21a)$$

with a cutoff frequency

$$f_{c, p_e} = c p_e \bigg/ \left\{2 d \frac{n_\perp}{n_{||}} \sqrt{n_{||}^2 - 1}\right\} \qquad (21b)$$

c is the free space light velocity.

The LSM modes excitation can also be examined in a similar manner. Consider the wavenumber to be α_{pm}, defined as $\alpha_{pm}^2 = \lambda^2 + \alpha^2$ and $\sqrt{n_\perp^2 - \alpha_{pm}^2} = k_{cm}/k_0$, $\sqrt{\alpha_{pm}^2 - 1} = h_m/k_0$, $u_{n1} = j k_{cm}/k_0$ and $u_0 = h_m/k_0$.

The LSM characteristic equation along with the relation between k_{cm} and h_m result in the following two simultaneous transcendental equations

$$-(k_{cm} d) \cot(k_{cm} d) = \mu_r(h_m d) \qquad (22a)$$

$$(k_{cm} d)^2 + (h_m d)^2 = \left(k_0 d \sqrt{n_\perp^2 - 1}\right)^2 = r_m^2. \qquad (22b)$$

The above equations can be graphically examined by plotting them in a $h_m d$ versus $k_{cm} d$ system. Again we have to recall the restriction $\text{Re}(u_0) \geq 0$, which means that valid solutions must satisfy $h_m \geq 0$. This condition can only be met when the radius of the circle (about the origin) defined by (22b) becomes larger than $\pi/2$, namely $r_m \geq \pi/2$. This fact gives the important result that there isn't any LSM surface wave excitation until the slab thickness becomes thick so that $r_m \geq \pi/2$. When the slab thickness increases even more, there is a possibility for higher-order LSM mode excitations. Their turn on condition is $r_m \geq (2q_m - 1)\pi/2$, where q_m is the LSM mode order. This mode can be expressed as

$$k_0 d \sqrt{n_\perp^2 - 1} \geq (2q_m - 1)\pi/2 \quad \text{where} \quad q_m = 1, 2, 3, \ldots \qquad (23)$$

The corresponding cutoff frequencies can then defined as

$$f_{c, q_m} = (2q_m - 1)c \bigg/ \left\{4 d \sqrt{n_\perp^2 - 1}\right\}. \qquad (24)$$

For the first LSM mode the cutoff frequency can be expressed in prescribed units as $f_{c, \text{LSM1}}(\text{GH}_z) = 75/\{d(\text{mm}) \sqrt{n_\perp^2 - 1}\}$.

Even more interesting expressions are the first LSM and the second LSE modes turn on conditions in terms of the normalized slab thickness d/λ

$$\text{LSM}_1 \text{ turn on:} \quad d/\lambda = 1 \bigg/ \left\{4 \sqrt{n_\perp^2 - 1}\right\} \qquad (25a)$$

$$\text{LSE}_2 \text{ turn on:} \quad d/\lambda = 1 \bigg/ \left\{2 \frac{n_\perp}{n_{||}} \sqrt{n_{||}^2 - 1}\right\}. \qquad (25b)$$

For example, considering a non-magnetic dielectric slab, the LSM_1 turn on condition for $\varepsilon_\perp = 9.6$ is $d/\lambda \geq 0.085$ and for

$\varepsilon_\perp = 13$ is $d/\lambda \geq 0.072$. Also, if $\varepsilon_\perp = 13$ and $\varepsilon_{||} = 10.2$ the LSE_2 turn on condition is $d/\lambda \geq 0.146$.

Summarizing, we can say that the first LSE mode is always excited. With an increase in the slab thickness, usually the first LSM can be turned on, followed by the second LSE mode.

During the numerical integration for the calculation of either the scattered field components or just the TEM reflection coefficient, the exact location of the surface wave poles α_{p_e} and α_{pm} is always needed. The most convenient manner to solve the characteristic equations is the use of iterative schemes, like the Newton-Raphson. These schemes always need a suitable starting value for the root to achieve fast convergence. For this reason the first mode wavenumbers are estimated by using the electrically thin substrate ($k_0 d \ll 1$) approximation, which gives

$$\left. \alpha_{p_e 1} \right|_{k_0 d \ll 1} \cong 1 + \frac{\mu_r (k_0 d)^2 (n_{||}^2 - 1)^2}{2 n_{||}^4}. \qquad (26)$$

The corresponding expression for the first LSM mode is

$$\left. \alpha_{pm 1} \right|_{k_0 d \ll 1} \cong \left\{ 1 + \left(\frac{1}{\mu_r k_0 d} \right)^2 \right\}^{1/2}. \qquad (27)$$

Of course, before attempting to solve for the roots, we first have to check if the corresponding turn on condition has been established.

IV. A THIN SUBSTRATE APPROXIMATION

The electrically thin substrate ($k_0 d \ll 1$) is often encountered in practical applications. Moreover, in applications such as wide microstrip lines and patch antennas the characteristic equations for the effective dielectric constant, the resonant frequency and the input impedance involve the above-developed reflection coefficient with multiple arguments. Therefore, the calculation of Γ_{TEM} must be effective and fast, which means that it cannot be achieved using numerical integration. So, a thin substrate approximation, in a manner similar to that of Kuester et al. [6], using a Mellin transform, is important. The closed form expressions obtained for the two integrals $\Delta(\alpha)$ and $f_e(\alpha)$ are given in [4].

In the general case of electrically thick substrate or when more accurate results are needed, this thin substrate approximation can be used as a first step in the solution of patch antennas transverse resonance characteristic equations.

V. INTEGRATION PATH AND EFFECTS OF SINGULARITY LOCATIONS

A numerical integration scheme to calculate the TEM reflection coefficient as a function of the substrate thickness is used. The involved integrals to be evaluated numerically are $\Delta(\alpha)$ and $f_e(-\sqrt{n_{||}^2 - \alpha^2})$, which appear in (15d) and (18). First, the integrand singularities must be defined and the integration contour must then be properly deformed to avoid them.

Both integrands possess a pair of branch cuts at $u_0 = 0$ or $\lambda = \pm j \sqrt{\alpha^2 - 1}$ as well as a set of LSE poles at $\lambda = \pm \lambda_e = \pm \sqrt{\alpha_{p_e}^2 - \alpha^2}$, where α_{p_e} is the corresponding

LSE mode wavenumber obtained from the solution of their characteristic equation. For the substrate thickness usually used in practical applications, only the first LSE mode is excited. The corresponding wavenumber $\alpha_{p_e 1}$ is calculated from the solution of the characteristic equation with a 10^{-6} error tolerance by using a Newton-Raphson technique.

The contribution of the pole located at $\lambda = \sqrt{n_{||}^2 - \alpha^2}$ to the f_e integral, has already been taken into account in (18) as a Cauchy principal value. For this last approach we have to keep in mind that an integration path along the real λ-axis is assumed. Also, we must take into account that the substrate is considered to be lossless, so that this pole lies on the real axis, otherwise it will be shifted to the lower complex λ-half plane.

Additionally, the integrand of the function $\Delta(\alpha)$ possess a pair of simple poles on the $\text{Im}(\lambda)$ axis at $\lambda = \pm j\alpha$. Moreover, if the substrate is thick enough then a set of LSM poles will also appear on the real axis at $\lambda = \pm \lambda_m = \pm \sqrt{\alpha_{pm}^2 - \alpha^2}$. Usually in practice none LSM mode is excited and only for quite thick substrates just the first one is turned on, according to the condition (23).

Furthermore, some terms are not singular (removable singularities) but they may cause numerical instabilities if they are not properly accounted for. Thus, in both integrands the term "$\tanh(k_0 d u_{n2})/u_{n2}$" in the limit when $u_{n2} \to 0$, must be replaced by its limiting value $k_0 d$. Similarly, the f_e integrand term $u_{n1} \cdot \coth(k_0 d u_{n1})$ at the limit $u_{n1} \to 0$ is replaced by $1/k_0 d$.

It is obvious that the location of the above singularities depends upon the value of the propagation constant along the y-axis $\alpha = n_{||} \sin(\varphi)$, where φ is the angle of incidence. Considering the usual practical case where the slab thickness is such that only LSE_1 is excited and keeping in mind that always $\alpha_{p_e 1} > 1$. We distinguish three cases for the singularity locations.

1) First case $\alpha_{p_e 1} < \alpha < n_{||}$: All singularities, except that of the f_e pole at $\lambda = \sqrt{n_{||}^2 - \alpha^2}$, are located on the $\text{Im}(\lambda)$ axis. Since, it is $\alpha > 1, u_0$ is purely real. From (2) we can see that the electromagnetic field in the air region decays exponentially, which means that there isn't any "sky wave radiation." Also, it has been proved by Chang et al. [5], that the surface wave propagating in the dielectric away from the open edge (area without upper conductor, negative x-direction) behaves as $\exp(k_0 \sqrt{\alpha^2 - \alpha_{p_e}^2} x)$. So, for the case $\alpha > \alpha_{p_e 1}$, it decays exponentially as it propagates away from the edge.

   Moreover, as can be seen in the next section, $X(\alpha)$ is real and consequently, the reflection coefficient magnitude becomes unity. This phenomenon corresponds to a total reflection and can be utilized to guide electromagnetic waves in the y-direction. Such an application is the study of wide microstrip lines.

2) Second case $1 < \alpha < \alpha_{p_e 1} < n_{||}$: Again there is no sky wave radiation since u_0 remains purely real and the corresponding branch cut lies on the $\text{Im}(\lambda)$ axis. The surface wave pole is moved on the $\text{Re}(\lambda)$ axis and
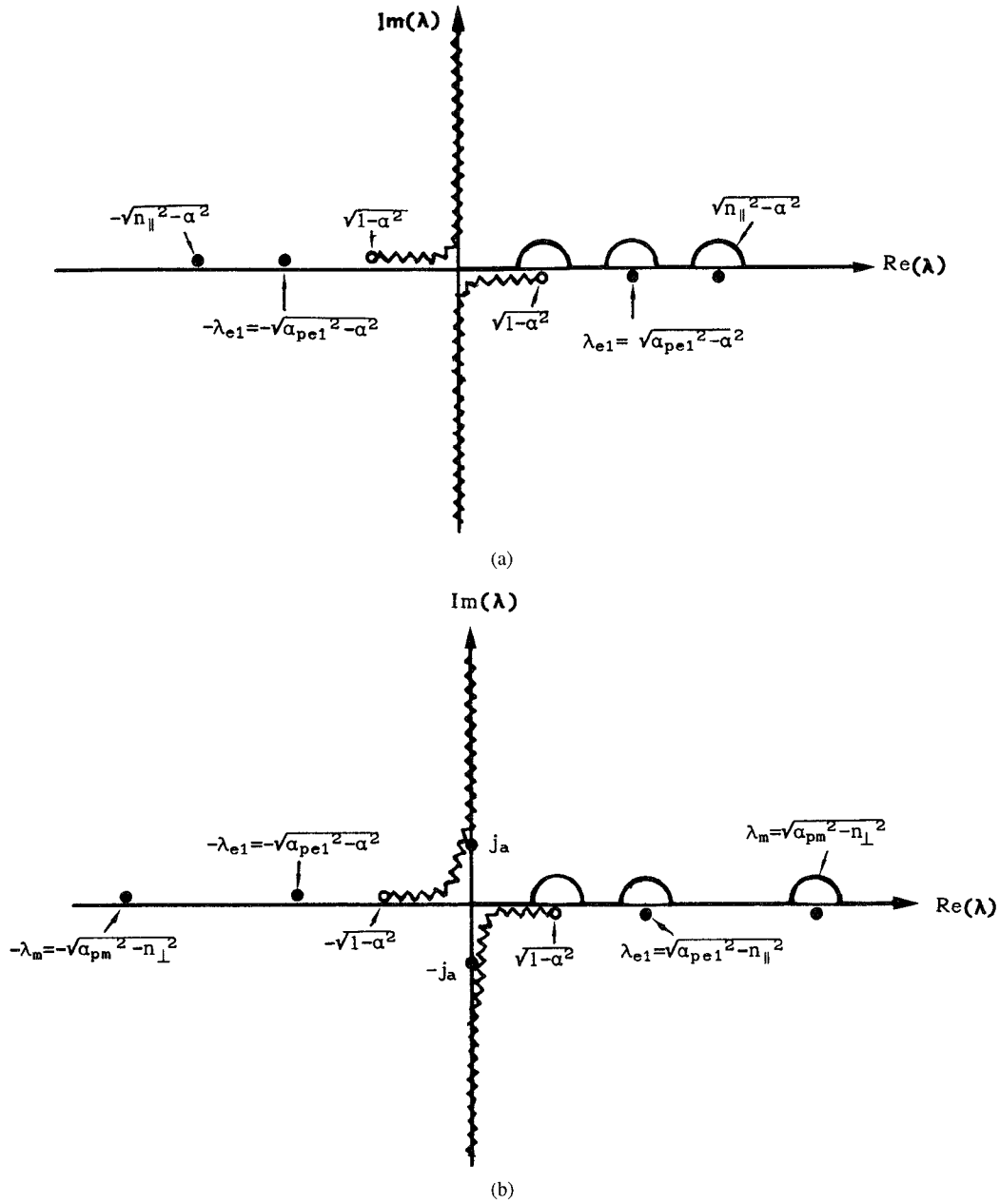
Fig. 2. Integration path for the third case $0 < \alpha < 1$. (a) Path for the integrand of function f_e. (b) Path for the integrand of function $\Delta(\alpha)$. The pole λ_m exists only for thick substrates, according to condition (27a).

the integration contour must be deformed to avoid it. A part of the incident energy will be propagated in the negative x-direction in the form of surface waves as $\exp(jk_0\sqrt{\alpha_{p_c}^2 - \alpha^2}\,x)$. Moreover, the function $X(\alpha)$ becomes complex and the magnitude of the reflection coefficient becomes less than unity.

3) Third case $0 < \alpha < 1$: In addition to the case 2) phenomena, sky wave radiation will occur. The term u_0 becomes purely imaginary (for a lossless substrate, but complex for a lossy one) and the corresponding branch cut $\lambda = \sqrt{1 - \alpha^2}$ is moved on the Re(λ) axis. Again the integration contour must be deformed to avoid this singularity. Due to the sky wave radiation the reflection coefficient decreases as $\alpha \rightarrow 0$ or equivalently as the

TEM wave tends towards the normal incidence.

The more complicated integration path occurs in the third case, for which the integration path and the singularity locations for the two integrals f_e and $\Delta(\alpha)$, can be seen in Fig. 2(a) and (b), respectively. The first two cases are simpler and can be easily deduced from the last one by considering the appropriate movement of singularities to the Im(λ) axis as described above.

VI. NUMERICAL INTEGRATION

The numerical integration of the complex integrals of f_e and $\Delta(\alpha)$ along the Re(λ) axis is carried out by using Romberg technique [11]. First, the singularities on the positive Re(λ) axis are located. Then, the integration path is divided into small

sections, especially on the neighborhood of the singularities. An adaptive Romberg integration is applied to each of these finite intervals with a 10^{-6} error tolerance. The integration is performed upto a point close to the singularity and continues from a point just after the singularity. Logarithmic singularities can be approached easier and more closely, because of the slowly varying nature of the logarithm. Considering λ_0 to be such a logarithmic singularity, the interval on one side is taken within the points $0.9\lambda_0$ and $(1 - 10^{-5})\lambda_0$ and the integration resumes on the other side from the point $(1 + 10^{-5})\lambda_0$ to $1.1\lambda_0$ and continues. On the other hand, functions are varying very fast at pole singularities, like f_e at the pole $\lambda_p = \sqrt{n_{||}^2 - \alpha^2}$. So, this pole must be approached gradually, while at the same time its location must be "exactly" determined. In the scheme used, λ_p is approached by intervals defined by the points $0.8\lambda_p, 0.99\lambda_p$ and $0.9999\lambda_p$ on one side and by $1.0001\lambda_p, 1.01\lambda_p$ and $1.2\lambda_p$ on the other side. In this manner the pole is approached to $10^{-4}\lambda_p$ and as we previously mentioned its location is estimated with a 10^{-6} tolerance. Also, the contribution on the pole itself is taken as a Cauchy principal value. Finally, some more intervals are taken as fractions of the $[0, \max(n_\perp, n_{||})]$ where the integrals contribution is expected to be more significant.

For the semi-infinite interval well beyond the singularities, a progressive Romberg integration is used. Namely, integration is performed on subintervals of length $1/k_0 d$, until the last subinterval contribution is less than 10^{-5}.

Even though the integration technique described in the last two sections refers to a lossless substrate, it can also be applied to lossy ones.

VII. NUMERICAL RESULTS AND DISCUSSIONS

The first LSE mode wavenumber $\alpha_{p_e 1}$ is calculated by using the value given in (26) as an initial guess. Since, $\alpha_{p_e 1}$ is always slightly greater than unity, it is better to plot $\alpha_{p_e 1} - 1$ as suggested in [9, p. 158]. In this manner, Fig. 3 shows a semilogarithmic plot of $(\alpha_{p_e 1} - 1)$ versus the normalized substrate thickness d/λ with the anisotropy ratio as a parameter. The curve for the isotropic case $n_x/n_z = 1$ and $\varepsilon_x = 9.6$ of Fig. 3(a) is in a very good agreement with the corresponding one given in [9]. An interesting observation in Fig. 3(a) is that keeping $\varepsilon_\perp = \varepsilon_x$ constant and varying $\varepsilon_{||} = \varepsilon_z$ we have a somewhat parallel shift of $\log(\alpha_{p_e 1} - 1)$ versus d/λ. Such a behavior is encountered also in the isotropic case [9] when ε_r is varied. Examining Fig. 3(b), where $\varepsilon_{||}$ is kept constant and $\varepsilon_\perp$ is varied, we can see that the anisotropy ratio affects $\alpha_{p_e 1} - 1$ only for thick substrates, while for thin substrates the three curves are coincided.

One of our first concerns was to check the validity of the thin substrate (th. subs.) approximation using the results from the numerical integration (num. int.). A case of an electrically thin substrate $d/\lambda = 0.01$ is shown in Fig. 4. In Fig. 4(a) the real part of $X(\alpha)$ or equivalently the phase of the reflection coefficient versus the propagation constant $\alpha = n_{||} \sin(\varphi)$ is plotted, with the anisotropy ratio as a parameter. The coincidence of the two sets of curves (th. subs. and num. int.) is obvious. The corresponding curves for the imaginary
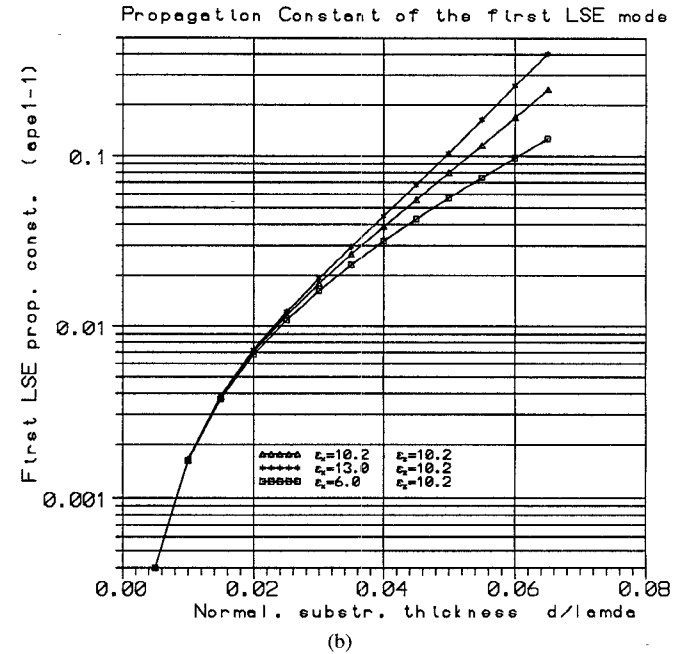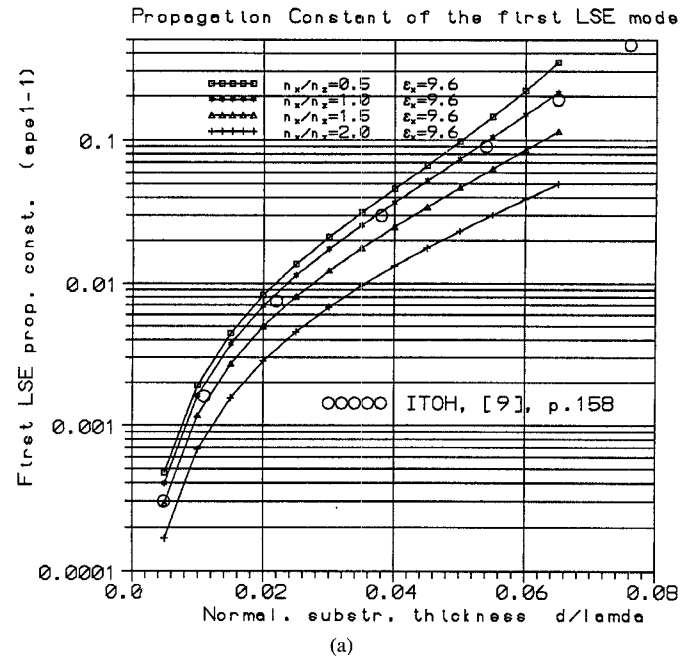

Fig. 3. Wavenumber of the first LSE mode $(\alpha_{p_e 1})$. Actually, $(\alpha_{p_e 1} - 1)$ versus the normalized substrate thickness d/λ. (a) Varying $\varepsilon_{||} = \varepsilon_z$ for constant $\varepsilon_\perp = \varepsilon_x = \varepsilon_y$. (b) Varying $\varepsilon_\perp = \varepsilon_x = \varepsilon_y$ for constant $\varepsilon_{||} = \varepsilon_z$.

part $\mathrm{Im}X(\alpha)$, which can give the magnitude of the reflection coefficient as $\exp\{\mathrm{Im}X(\alpha)\}$, are shown in Fig. 4(b). It can be seen that the anisotropy ratio has no effect in this case. There is a small deviation between th. subs. approximation and num. int. results only for small values of α (near normal incidence, $\alpha \to 0$).

In order to further examine the reflection coefficient behavior with respect to the slab thickness and also to define the limits of the th. subs. approximation, we have calculated and plotted both its magnitude and phase versus the normalized substrate thickness d/λ for some constant values of the propagation constant α. In Fig. 5 the $\varepsilon_{||}$ is kept constant varying
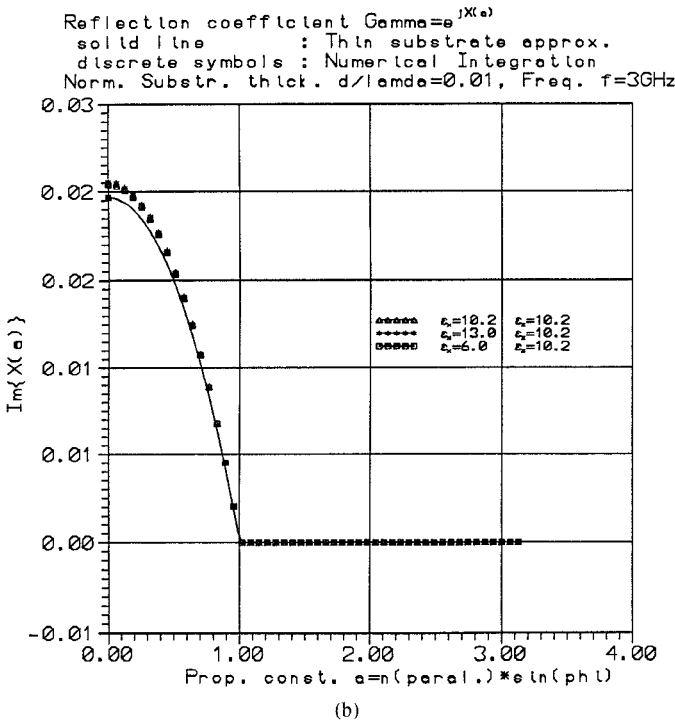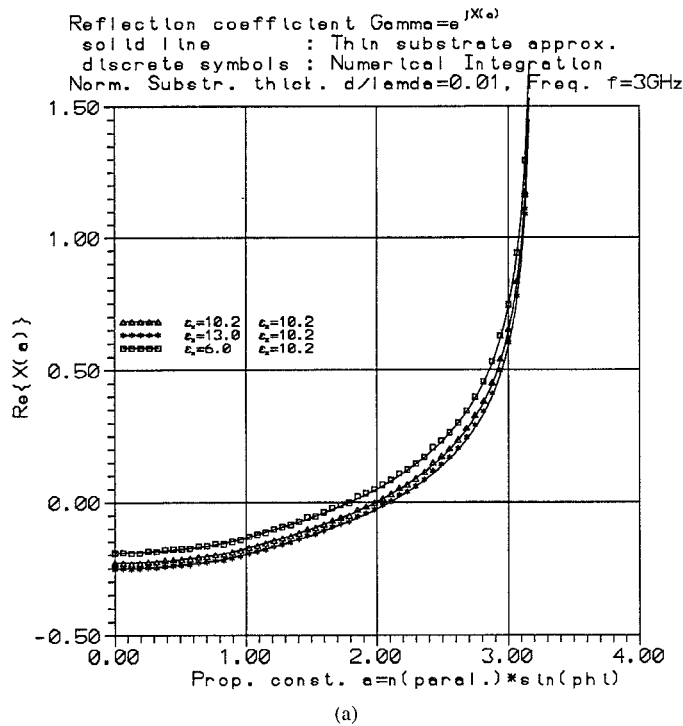
Fig. 4. Influence of the dielectric anisotropy on the reflection coefficient $\Gamma(\alpha)$ and comparison of the thin substrate approximation and numerical integration for $d/\lambda = 0.01$. (a) $\mathrm{Re}\{X(\alpha)\}$ or the phase of the reflection coefficient. (b) $\mathrm{Im}\{X(\alpha)\}$, which gives the magnitude of the reflection coefficient.

Fig. 5. Reflection coefficient $\Gamma(\alpha)$ versus the substrate thickness d/λ, with $\alpha = n_{||} \sin(\varphi) = 0.5$, for constant $\varepsilon_{||} = \varepsilon_z$ and varying $\varepsilon_{\perp} = \varepsilon_x = \varepsilon_y$. (a) $\mathrm{Re}\{X(\alpha)\}$ or the phase of the reflection coefficient. (b) $\mathrm{Im}\{X(\alpha)\}$, which gives the magnitude of the reflection coefficient.

the $\varepsilon_{\perp}$ used as a parameter, while variations are done vice versa in Fig. 6.

Examining Figs. 5(a) and 6(a) for the phase of the reflection coefficient $\mathrm{Re}X(\alpha)$ a fairly good agreement between th. subs. approximation and num. int. results can be obtained for thin substrates. The deviation between them is less than 8% for substrate thickness upto $d/\lambda = 0.04$, but it is then increased
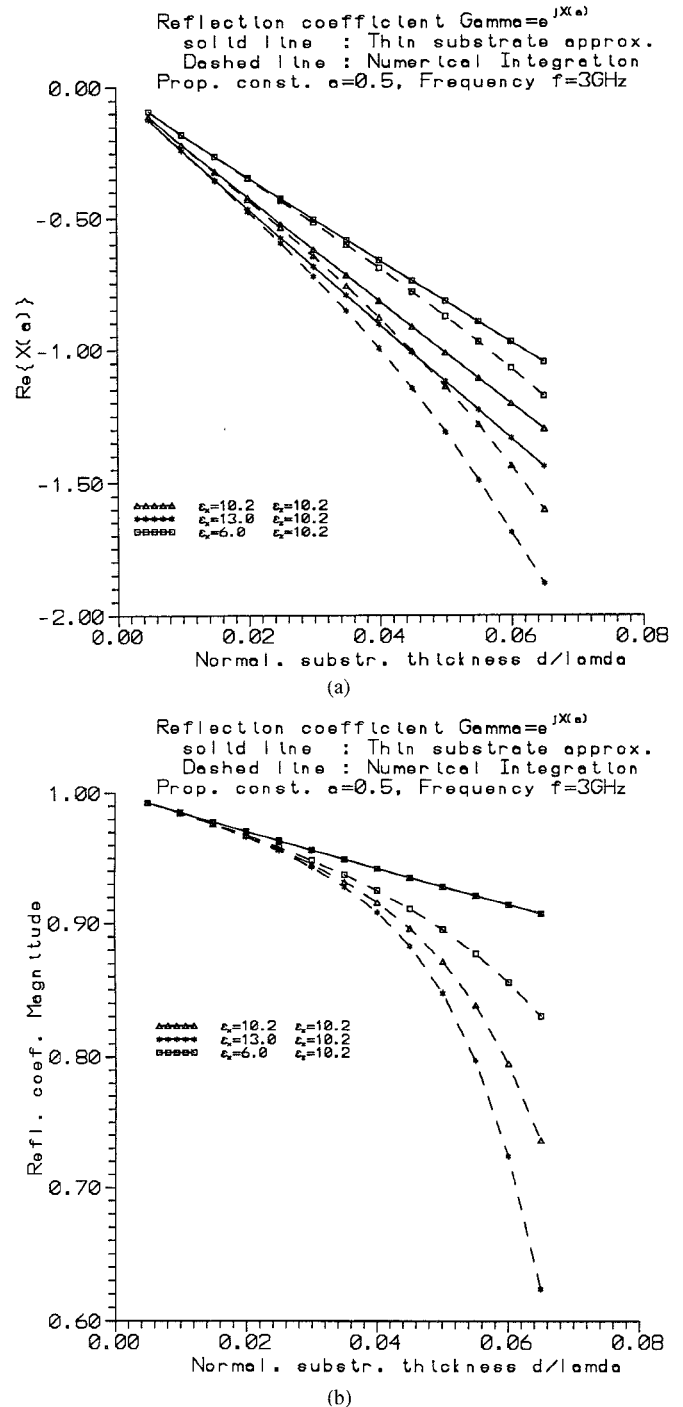
and at $d/\lambda = 0.065$ becomes 23% for Fig. 5(a) and 13% for Fig. 6(a). Concerning the magnitude of the reflection coefficient [see Figs. 5(b) and 6(b)], we received a significant deviation between the two approaches. At $d/\lambda = 0.04$ it reaches 35% in Fig. 5(b) and 22% in Fig. 6(b). In, fact the th. subs. approximation fails to account for variations in the dielectric constant $\varepsilon_{\perp} = \varepsilon_x = \varepsilon_y$ parallel to the ground plane [Fig. 5(b)], while it does follow the variations in $\varepsilon_{||} = \varepsilon_z$ normal to the ground plane, even though the deviation for
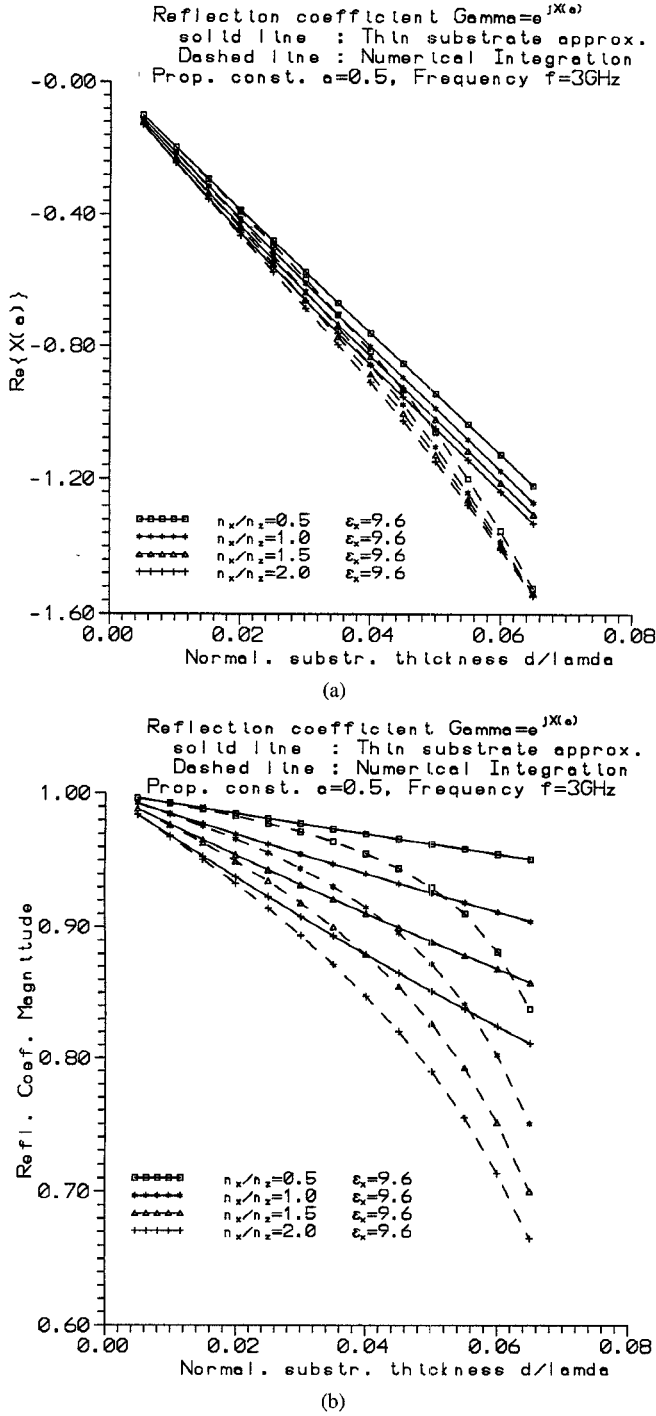
Fig. 6. Reflection coefficient $\Gamma(\alpha)$ versus the substrate thickness d/λ, with $\alpha = n_{||} \sin(\varphi) = 0.5$, for constant $\varepsilon_\perp = \varepsilon_x = \varepsilon_y$ and varying $\varepsilon_{||} = \varepsilon_z$. (a) Re$\{X(\alpha)\}$ or the phase of the reflection coefficient. (b) Im$\{X(\alpha)\}$, which gives the magnitude of the reflection coefficient.

thick substrate is still significant [Fig. 6(b)]. Moreover, the deviation between th. subs. approximation and num. int. seems to increase monotonically with $\varepsilon_\perp$ starting from $\varepsilon_\perp = 1$.

Furthermore, a monotonic decrease of the reflection coefficient magnitude [Figs. 5(b) and 6(b)] as a function of an increasing slab thickness is observed. This is just the expected behavior, since more energy will be radiated through the edge opening as the substrate gets thicker. A similar behavior is observed when $\varepsilon_\perp$ is increased, as shown in Fig. 5(b).

Moreover, a similar behavior of the reflection coefficient phase versus d/λ and $\varepsilon_\perp$ can be deduced from Figs. 5(a) and 6(a). This phase reduction could make impossible the establishment of transverse resonance conditions in microstrip structures. For example, the phase could remain negative for all possible values of the propagation constant ($\alpha = 0$ to $n_{||}$), as we have found for the case: $n_x/n_z = 2$ and $\varepsilon_x = 9.6$ (which gives $\varepsilon_{||} = 2.4$).

An example showing the dependence of the real (conductance G_e) and imaginary (susceptance) part of the normalized edge admittance Y_e/Y_0 from the normalized substrate thickness d/λ, appears in Fig. 7(a) and (b), respectively. The absolute values of G_e and B_e can be deduced from these curves by recalling the expression of $Y_0 = n_{||}/(\mu_r \zeta_0 d)$. For these curves we have $\mu_r = 1$, $\varepsilon_{||} = 10.2$, $f = 3$ GHz and $G_e = 0.0847 \cdot \text{Re}(Y_e/Y_0)/(d/\lambda)$. Similarly for B_e we use the Im(Y_e/Y_0) instead of the Re part. The effects of the dielectric anisotropy on the edge admittance are quite similar to the above described for the phase and the magnitude of the reflection coefficient.

The above observations and conclusions could be used as a guide in applying this reflection coefficient in the analysis of microstrip lines and patch antennas printed on uniaxial substrate.

The phase of the reflection coefficient Re$X(\alpha)$ is involved in the estimation of the propagation constants or the resonant frequencies by establishing transverse resonance conditions. This task requires the solution of transcendental characteristic equations, which in turn involves the reflection coefficient and in some cases more than once with different arguments (i.e. triangular patch antennas). Since the th. subs. approximation behaves quite well for the Re$X(\alpha)$, even at its worst case with thick substrate and large $\varepsilon_\perp$ it can be used without any serious doubts within the solution of such equations. In the case when better accuracy is required or when d/λ and $\varepsilon_\perp$ are large, the th. subs. approximation must be used first to get a solution quite close to the actual one. Afterwards a solution scheme employing numerical integration for $X(\alpha)$ should be used to improve the accuracy of the solution. In this manner time consuming calculations which require the iterative use of numerical integration are kept at a minimum.

The magnitude of the reflection coefficient is involved in the calculations of the normalized edge admittance, the normalized radiated power $(1 - |\Gamma|^2)$ and the input impedance of patch antennas. Since these quantities are usually calculated only once at each frequency (or for a specified set of input data) and significant deviations in $|\Gamma|$ values between th. subs. approximation and num. integration are observed, the use of the numerical integration in the case of thick substrates is strongly recommended. In the case of electrically thin substrates $(d/\lambda \leq 0.02)$ the th. subs. approximation can be safely used with an error less than 8%.

VIII. CONCLUSION

A Wiener-Hopf-type solution of the canonical problem of a TEM wave falling upon the edge of the truncated upper conductor of a grounded uniaxial anisotropic dielectric
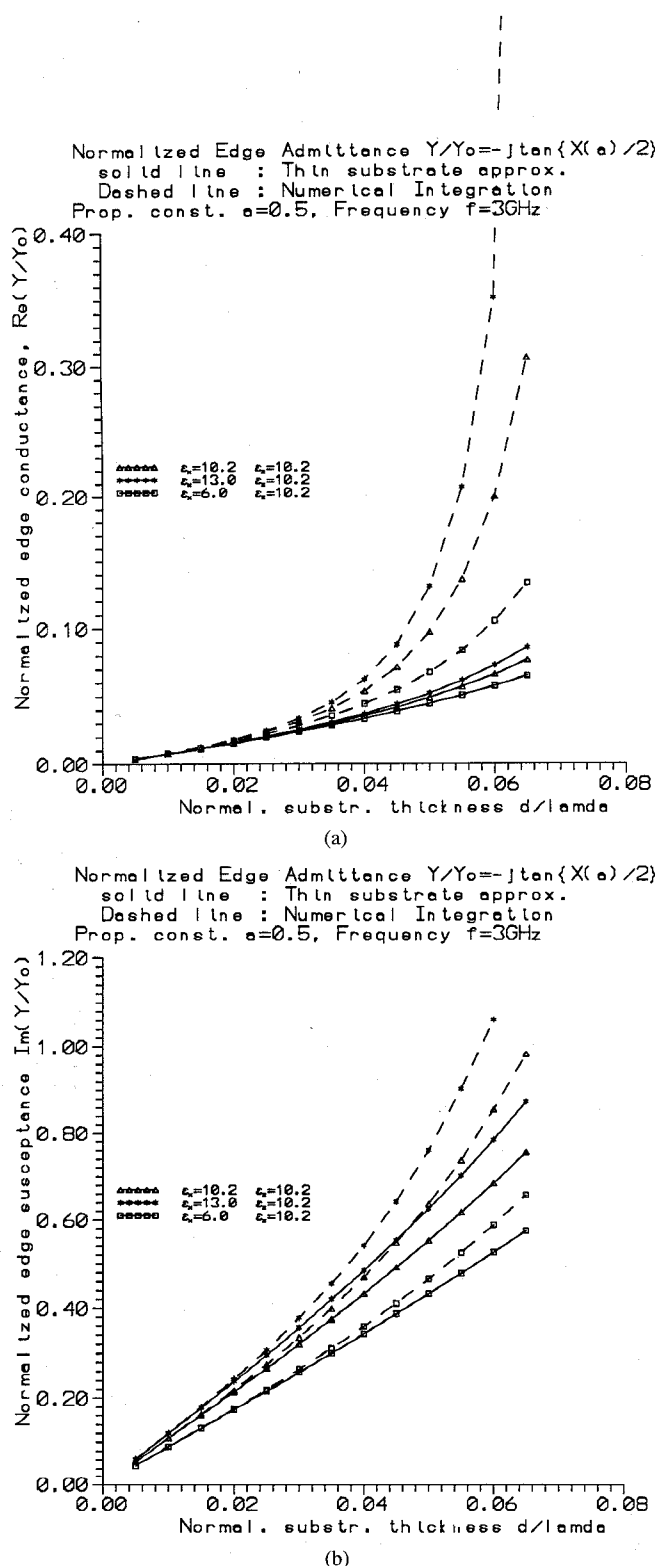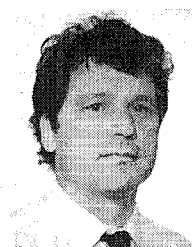
reflection coefficient are evaluated numerically and the limits of the relevant thin substrate approximation are established. Numerical results show that there are significant effects of the dielectric anisotropy, which in some cases can be accounted for only by using numerical integration. Either the thin substrate approximation or the numerical evaluation for the reflection coefficient can be used in wide microstrip lines and patch antenna applications. Recommendations on their use are also given, based on parametric investigations by varying the dielectric anisotropy characteristics and the slab thickness.

REFERENCES

[1] N. G. Alexopoulos, "Integrated circuit structures on anisotropic substrates," *IEEE Trans. Microwave Theory Tech.*, vol. MTT-33, pp. 847–881, Oct. 1985.

[2] D. M. Pozar, "Radiation and scattering from a microstrip patch on a uniaxial substrate," *IEEE Trans. Microwave Theory Tech.*, vol. AP-35, pp. 613–621, June 1987.

[3] R. M. Nelson, D. A. Rogers, and A. G. D'Assuncao, "Resonant frequency of a rectangular microstrip patch antenna on several uniaxial substrates," *IEEE Trans. Antennas Propagat.*, vol. 38, pp. 973–981, July 1990.

[4] G. A. Kyriacou and J. N. Sahalos, "The edge admittance model for the study of microstrips on uniaxial substrate," in *Archiv fur Electrotechnik 76.* New York: Springer, 1993, pp. 169–179.

[5] D. C. Chang and E. F. Kuester, "Total and partial reflection from the end of a parallel-plate wave waveguide with an extended dielectric slab," *Radio Sci.*, vol. 16, no. 1, pp. 1–13, 1981.

[6] E. F. Kuester, R. T. Johnk, and D. C. Chang, "The thin substrate approximation for reflection from the end of a slab-loaded parallel-plate wave waveguide with application to microstrip patch antennas," *IEEE Trans. Antennas Propagat.*, vol. AP-30, pp. 910–917, Sept. 1982.

[7] Y. Tu and D. C. Chang, "Effects of a cover layer on the edge admittance of a wide microstrip," *IEEE Trans. Antennas Propagat.*, vol. 39, pp. 354–358, Mar. 1991.

[8] R. Mittra and S. W. Lee, *Analytical Techniques in the Theory of Guided Waves.* New York: McMillan, 1971.

[9] J. R. Mosig, "Numerical techniques for microwave and millimeter wave passive structures," in *Integral Equation Techniques*, T. Itoh, Ed., ch. 3. New York: Wiley, 1989.

[10] D. M. Pozar, *Microwave Engineering.* Reading, MA: Addison-Wesley, 1990.

[11] G. Dahlquist and A. Bjorsk, *Numerical Methods.* Englewood Cliffs, NJ: Prentice-Hall, 1974.

[12] K. L. Wong, J. S. Row, C. W. Kuo, and K. C. Huang, "Resonance of a rectangular microstrip patch antenna on a uniaxial substrate," *IEEE Trans.*, vol. 41, pp. 698–701, Apr. 1993.

[13] S. S. Toncich, R. E. Collin and K. B. Bhasin, "Full-wave characterization of microstrip discontinuities patterned on anisotropic substrates, using potential theory," *IEEE Trans. Microwave Theory Tech.*, vol. 41, pp. 2067–2073, Dec. 1993.

[14] C. Peixeiro and A. M. Barbosa, "Leaky and surface waves in anisotropic printed antenna structures," *IEEE Trans. Antennas Propagat.*, vol. 40, pp. 566–569, May 1992.

[15] G. A. Kyriacou and J. N. Sahalos, "Effects of substrate—superstrate anisotropy on microstrip structures," *Electron. Lett.*, vol. 30, no. 19, pp. 1557–1558, Sept. 15, 1994.

Fig. 7. Normalized edge admittance Y_e/Y_0 versus the substrate thickness d/λ, with $\alpha = n_{||}\sin(\varphi) = 0.5$, for constant $\varepsilon_{||} = \varepsilon_z$ and varying $\varepsilon_\perp = \varepsilon_x = \varepsilon_y$. (a) $\mathrm{Re}\{Y_e/Y_0\}$ or normalized edge conductance G_e/Y_0. (b) $\mathrm{Im}\{Y_e/Y_0\}$ or normalized edge susceptance B_e/Y_0.

slab is first summarized. The surface waves characteristic equations are investigated and explicit expressions for the LSE and LSM modes turn on conditions are given. The Sommerfeld-type integrals involved in the expression of the

George A. Kyriacou (M'90) was born in Famagusta, Cyprus on March 25, 1959. He received the Electrical Engineering Diploma in 1984 and the Ph.D. degree in 1988, both with honors, from Demokritos University of Thrace.

Since January 1990 he was a Lecturer at the Microwaves Laboratory of the same University, where now is an Assistant Professor. His current research interests include microwave engineering, antennas, applied electromagnetics, and biomedical engineering. He works on electrical impedance tomography, participating in several European Union programs.

Dr. Kyriacou is a member of the Technical Chamber of Greece.
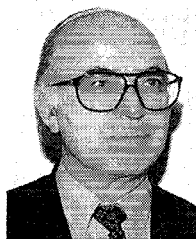
John N. Sahalos (M'75-SM'84) was born in Philippiada, Greece, in November, 1943. He received the B.Sc. degree in physics and the Diploma in civil engineering from the University of Thessaloniki, Greece, in 1967 and 1975, respectively, and the Diploma of Post-Graduate Studies in electronics in 1975 and the Ph.D. in electromagnetics in 1974.

From 1971 to 1974 he was a Teaching Assistant of Physics at the University of Thessaloniki and was an Instructor there from 1974 to 1976. During 1976 he worked at the ElectroScience Laboratory, The Ohio State University, Columbus, as a Postdoctoral University Fellow. From 1977–1985 he was a Professor in the Electrical Engineering Department, University of Thrace, Greece, and Director of the Microwaves Laboratory. During 1982, he was a Visiting Professor at the Department of Electrical and Computer Engineering, University of Colorado, Boulder. Since 1985 he has been a Professor at the School of Science, University of Thessaloniki, Greece, where he is the leader of the Radiocommunications Group. During 1989 he was a Visiting Professor at the Universidat Politechnica de Madrid, Spain. His research interests are in the area of applied electromagnetics, antennas, high frequency methods, communications, microwaves, and biomedical engineering. He is the author of three books and more than 190 articles published in the scientific literature. He is a professional Engineer and a consultant to industry.

Dr. Sahalos has been honored with the Investigation Fellowship of the Ministerio de Education Y Ciencia (Spain). Since 1985 he has been a member of the Editorial Board of the IEEE TRANSACTIONS ON MICROWAVE THEORY AND TECHNIQUES. Since 1992 he has been a member of the URSI Commissions A and E. He is also a member of five IEEE Societies, of the New York Academy of Science, and of the Technical Chamber of Greece.